

HybriMap: Hybrid Clues Utilization for Effective Vectorized HD Map Construction

Chi Zhang¹, Qi Song¹, Feifei Li¹, Yongquan Chen² and Rui Huang¹

¹The Chinese University of Hong Kong, Shenzhen

²Shenzhen Institute of Artificial Intelligence and Robotics for Society

{chizhang1, qisong, feifeili1}@link.cuhk.edu.cn, {yqchen, ruihuang}@link.cuhk.edu.cn,

Abstract

Constructing vectorized high-definition maps from surround-view cameras has garnered significant attention in recent years. However, the commonly employed multi-stage sequential workflow in prevailing approaches often leads to the loss of early-stage information, particularly in perspective-view features. Usually, such loss is observed as an instance missing or shape mismatching in the final birds-eye-view predictions. To address this concern, we propose a novel approach, namely **HybriMap**, which effectively exploits clues from hybrid features to ensure the delivery of valuable information. Specifically, we design the Dual Enhancement Module, to enable both explicit integration and implicit modification under the guidance of hybrid features. Additionally, the perspective keypoints are utilized as supervision, further directing the feature enhancement process. Extensive experiments conducted on existing benchmarks have demonstrated the state-of-the-art performance of our proposed approach.

1 Introduction

The vectorized High-Definition (HD) map construction under Birds-Eye View (BEV) has been widely investigated in recent autonomous driving studies, due to the extensive demand in motion panning [Jian *et al.*, 2019; Diaz-Diaz *et al.*, 2022] and forecasting [Gao *et al.*, 2020; Da and Zhang, 2022; Conde *et al.*, 2023]. In particular, vectorized HD maps represent static map elements, such as pedestrian crossing, lane divider, and road boundaries, using parametric curves [Qiao *et al.*, 2023] or 2D vectors [Li *et al.*, 2022; Liu *et al.*, 2023; Liao *et al.*, 2022; Ding *et al.*, 2023; Liao *et al.*, 2023], providing notable benefits in terms of scalability and storage consumption. In this paper, we continue representing map elements in 2D vectors and direct our efforts toward enhancing the precision and reliability of vectorized HD map construction.

Given the fact that input images and output map predictions exist in separate coordinate systems, existing HD map construction methods, such as HDMaNet [Li *et al.*, 2022], VectorMaNet [Liu *et al.*, 2023], and MapTRv2 [Liao *et al.*,

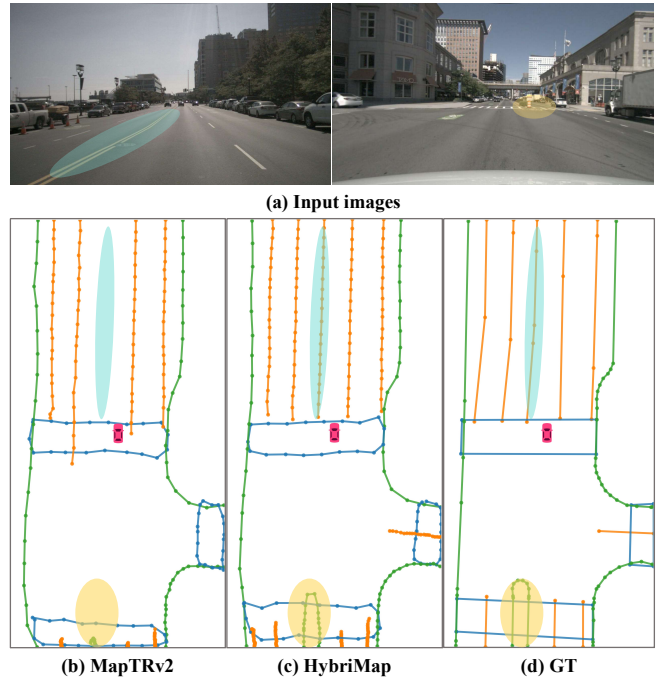


Figure 1: **Hard cases in HD map construction.** MapTRv2[Liao *et al.*, 2023] tends to lose specific instance clues or shape priors existing in the input images, as visualized in (b). In the proposed HybriMap, we can well maintain the given priors and thus strengthen the alignment between the original input and map prediction, by employing a hybrid approach.

2023], typically employ a sequential workflow incorporating multi-stage processes: 1) an image backbone network to extract perspective-view (PV) features from input images; 2) a cross-view transformation network to project PV features into the birds-eye view; 3) a transformer-based BEV decoder to generate the final map predictions. However, the sophisticated nature of the cross-view transformation network introduces a significant challenge in terms of early-stage data loss, specifically the PV features. Taking MapTRv2 as an example, such a prior loss problem is often observed as the discrepancies between the input PV images and the final map predictions, as presented in Fig.1 (b). For instance, the lane divider highlighted in the blue area is visible in the left im-

age but fails to be detected in the MapTRv2. Additionally, the road boundary indicated by the yellow circle appears to extend beyond the crossing in the right image but is mispredicted as a small instance by MapTRv2.

Intuitively, the aforementioned issue of early-stage data loss can be effectively addressed by reusing PV features that are full of spatial priors. Nevertheless, it is worth noting that PV features often contain a large amount of redundant information from irrelevant categories like the sky and buildings, as only map elements are necessary for BEV map prediction. Conversely, despite the BEV representations produced by the cross-view transformation network suffering from prior loss, they still prioritize and highlight more meaningful and intricate elements compared to PV features. Consequently, a new question arises: How can we efficiently preserve the genuinely useful clues contained within both PV and BEV features?

We found that both PV feature and BEV feature can serve as valuable references or complementary sources of each other during feature enhancement. This motivates us to propose the **Hybrid** approach of HD Map construction (**HybriMap**), which involves a parallel channel to implement comprehensive and adequate exploitation of features from both PV and BEV into effective HD map construction. Specifically, we design a Dual Enhancement Module (DEM) to achieve feature enhancement through both explicit integration of hybrid features, and implicit upgrading of BEV features. The explicit branch of the DEM fuses features from both perspectives to capture an Integrated Positional Embedding and assist the subsequent decoding. Simultaneously, the implicit branch of the DEM focuses on emphasizing the valuable clues within the BEV features, taking advantage of the preceding fusion process that extracts the most worthwhile portions from the BEV features. This dual approach ensures a comprehensive and effective enhancement of the overall feature set.

Unlike the previous sequential workflow, which heavily depends on BEV representation, our proposed HybriMap leverages hybrid features to their fullest extent, addressing the issue of early-stage information loss. As illustrated in Fig.1 (c), HybriMap demonstrates its ability to preserve the initial priors from the original images and efficiently convert them into vectorized map instances, surpassing the performance of sequential pipelines like MapTRv2.

The contributions of this work are as follows:

- We propose a Hybrid approach, which enables the reutilization of PV features and interaction between features from both perspectives in vectorized HD map construction.
- We introduced the Dual Enhancement Module (DEM) that sufficiently leverages hybrid information through explicit integration and implicit upgrading.
- Our approach exhibits state-of-the-art results on the existing benchmarks, particularly with a notable improvement of 3.9% *mAP* on *nuScenes* dataset.

2 Related Work

2.1 Vectorized HD Map Construction

HMapNet [Li *et al.*, 2022] involves a post-processing procedure into the semantic segmentation and instance embedding, enabling the map to represent static elements in a vectorized form. Subsequent studies commonly employ the end-to-end networks to attain HD map construction. Several methods use the Bezier curve to represent map instances and predict HD map via parametric curve estimation [Can *et al.*, 2022; Qiao *et al.*, 2023]. One alternative is to represent map elements as 2D vectors. VectorMapNet [Liu *et al.*, 2023] structures the map construction as a vector detection problem. MapTR [Liao *et al.*, 2022] completes the map vector representation and refines the overall detection pipeline in a more concrete manner. Recent methods [Ding *et al.*, 2023; Yu *et al.*, 2023; Liao *et al.*, 2023; Yuan *et al.*, 2024] generally follow the conventional sequential process of 1) PV feature extraction, 2) BEV feature transformation, and 3) map vector prediction.

However, map predictions through the sequential process are vulnerable to early-stage information loss. Differently, we propose a novel Hybrid approach that re-utilizes PV features based on the hybrid of PV and BEV features, to address the issue of information loss that commonly occurs in traditional pipelines.

2.2 Cross-View Information Utilization

The utilization of cross-view information is a typical topic in the map-learning area. PyOccNet [Roddick and Cipolla, 2020] transforms PV features into BEV through a pyramid network, preserving multi-scale information from inputs. The existing Cross-view Transformation [Yang *et al.*, 2021] activates the mutual response between cross-view features, to enhance the feature in the objective domain. Zhou *et al.* [Zhou and Krähenbühl, 2022] involve image-view features and camera-aware embedding in the implementation of segmentation under map-view. BEVFormerV2 [Yang *et al.*, 2023] simply performs post-processing and encoding on PV features and thus enhances the network’s decoding capability for BEV features. ScalableMap [Yu *et al.*, 2023] employs a fusion module on two branches originating from PV features to enhance the BEV features.

In our HybriMap, we design the Dual Enhancement Module, where the implicit and explicit cross-view utilization are coupled. DEM simultaneously activates the implicit enhancement of BEV representation and elevates the decoding performance of map predictions through explicit aggregation of hybrid features.

3 Method

3.1 Architecture Overview

The pipeline of HybriMap is depicted in Fig. 2. Given a set of RGB images $\{I_i \in \mathbb{R}^{H_I \times W_I \times 3}, i = 1, 2, \dots, N\}$ from N cameras, HybriMap aims to predict N_m map instances on N_c classes in the form of vectors with N_p points $\{\hat{v}_i \in \mathbb{R}^{N_p \times 2}, i = 1, 2, \dots, N_m\}$ and the classification scores $\{\hat{c}_i \in \mathbb{R}^{N_c \times 1}, i = 1, 2, \dots, N_m\}$ eventually.

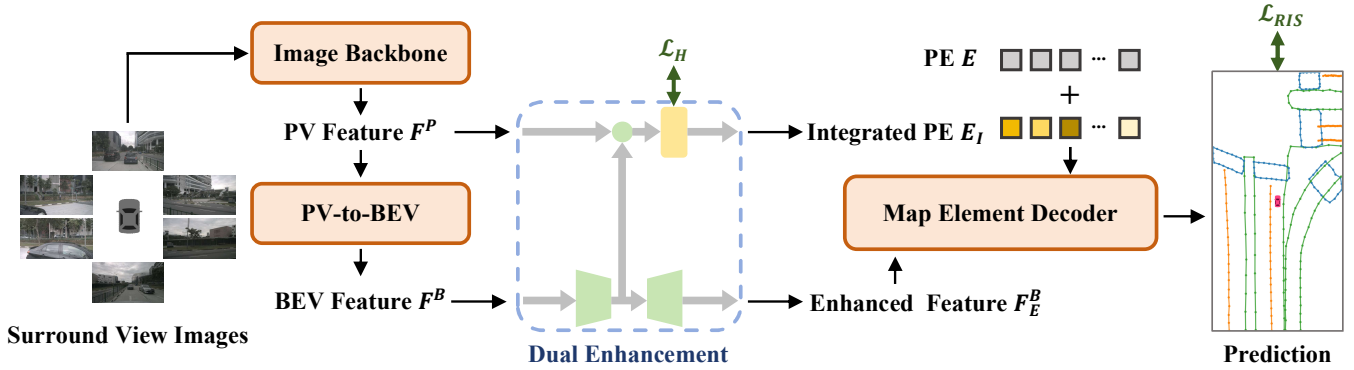


Figure 2: **The overall architecture of HybriMap.** The DEM is depicted in an abstract version. "L" indicates that the outputs are supervised by the corresponding loss, and "PE" means positional embedding. Different from the typical sequential workflow, the proposed method leverages a Hybrid approach that deeply exploits features from both PV and BEV. Such an approach enhances the reliance of the prediction results on the original information, thereby mitigating the negative impacts of early-stage information loss.

Image Backbone. The input images are sent into the image backbone and converted to PV features $\{F_i^P \in \mathbb{R}^{H_F \times W_F \times C_F}, i = 1, 2, \dots, N\}$. By default, we adopt ResNet [He *et al.*, 2016] as the image backbone.

PV-to-BEV. The PV-to-BEV module further transforms the PV features into BEV features $F^B \in \mathbb{R}^{H \times W \times C}$. LSS transform [Phillion and Fidler, 2020] is employed to be the default method.

Dual Enhancement Module. In the Dual Enhancement Module, the hybrid features consisting of PV features F^P and BEV features F^B are utilized as inputs. Specifically, F^P and F^B are fused to generate Integrated Heatmap H^P , which is then converted into Integrated Positional Embedding E_I . B is synchronously updated as implicitly enhanced BEV feature F_E^B . The thorough purpose and operation of DEM will be introduced in Sec. 3.2.

Map Element Decoder. Outputs from DEM, i.e. E_I and F_E^B are then transferred into a transformer-based map element decoder. We leverage the transformer-based decoder [Carion *et al.*, 2020; Zhu *et al.*, 2020] to directly output the prediction results. Specifically, we adopt hierarchical query Q [Liao *et al.*, 2022] and enhanced BEV features F_E^B as the query and value of the decoder, respectively. The positional embedding used in the decoder is combined by the globally applicable learnable positional embedding [Gehring *et al.*, 2017], and the Integrated Positional Embedding E_I that is relevant to the hybrid features. The decoder directly predicts N_m map elements, containing coordinates \hat{v} and classification score \hat{c} of the vectors.

Losses. We propose Heatmap Loss \mathcal{L}_H to constrain the enhancement effects of DEM. Additionally, Rasterized Instance Segmentation (RIS) Loss \mathcal{L}_{RIS} is introduced to further improve the prediction performance. The details of the loss components are further discussed in Sec.3.3.

3.2 Dual Enhancement Module

The Dual Enhancement Module is designed for the deep exploitation of hybrid features, as depicted in Fig. 3. The valu-

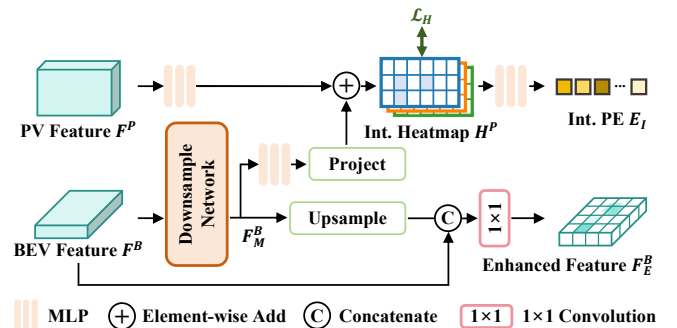


Figure 3: **Workflow of the Dual Enhancement Module.** Given the hybrid information, Integrated Positional Embedding explicitly incorporates features from both perspectives, where the intermediate Integrated Heatmap is supervised. BEV features, based on the extracted useful portion among itself, are thereby implicitly enhanced. The dual enhancement enables the sufficient and effective utilization of hybrid information.

able priors within the hybrid features are explicitly integrated and formed as position embedding. To facilitate the efficacy, a crucial intermediate, i.e., Integrated Heatmap, is supervised. Additionally, the extracted refined BEV features are further leveraged for the implicit enhancement of themselves. Such enhancement highlights the genuinely useful portions within the hybrid information and guides the subsequent decoding process.

Integrated Positional Embedding

The PV and BEV information is explicitly incorporated to generate the Integrated Positional Embedding in this branch of DEM. According to the design of the map decoder [Zhu *et al.*, 2020], the positional embedding serves not only as a decorative element for the input information but also plays a role in generating reference points, which serve as the initial estimates of the map vectors. By incorporating hybrid features into the positional embedding, the decoded feature representation and vector estimation become more receptive to the cues derived from the hybrid information, as evident from

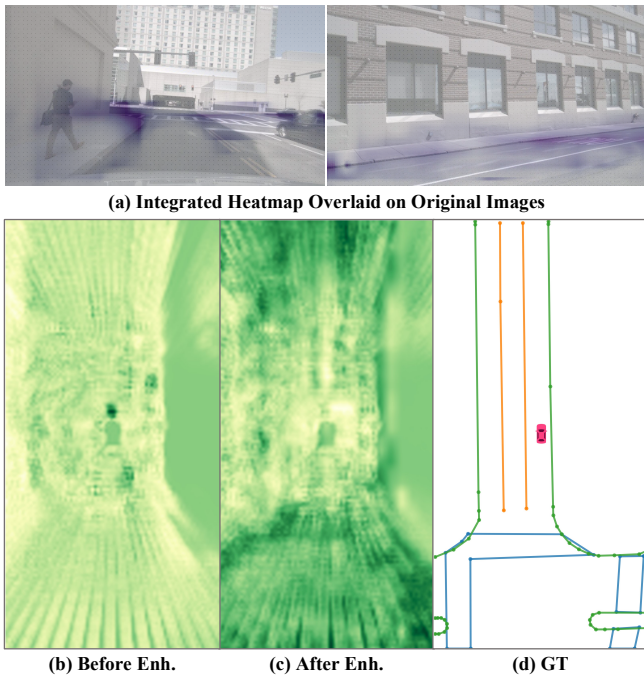


Figure 4: **Illustration of Integrated Heatmap and BEV Enhancement.** "Enh." indicates the implicit enhancement process on the BEV features. As presented in (a), the integrated heatmap gathers higher heat intensities around the crucial map instances, e.g. pedestrian crossing and road boundaries. Additionally, the second row shows the BEV feature maps before and after implicit enhancement. It is evident that the original BEV features in (b) basically depict the distinction of the drivable area, whereas the enhanced BEV features in (c) accentuate the details near map instances.

the functional implications of the positional embedding.

Suppose $\Psi^n(\cdot)$ is the convolution network function connected with n cascaded layers. We first downsample F^B into the BEV Enhancement Map F_M^B from BEV features by multi-layer convolution:

$$F_M^B = \Psi^3(F^B) \quad (1)$$

where $F_M^B \in \mathbb{R}^{(H/d) \times (W/d) \times C}$, d is the pre-defined down-sample scale factor.

F_M^B is then projected into perspective-view. For an arbitrary coordinate (x, y) in the BEV plane, we first complete it to a 3D coordinates (x, y, z) by assigning a constant height value. Given the camera parameter matrix \mathbf{P} , the coordinate (x, y, z) in the 3D camera ego space can be converted to pixel (u, v) in the image coordinate by the following relationship:

$$[u, v, 1]^T = \mathbf{P} \times [x, y, z, 1]^T \quad (2)$$

We create a perspective-view feature map for each class, denoted as $F_M^P \in \mathbb{R}^{H_I \times W_I \times N_c}$ and initialize it to be blank. The BEV Enhancement Map F_M^B generated from Eq.1 is firstly encoded by multilayer perceptron (MLP) and projected by assigning feature values to the corresponding region:

$$F_M^P[u, v, c^{id}] = MLP(F_M^B)[x, y, c^{id}] \quad (3)$$

in which the relationship between (u, v) and (x, y) is illustrated in Eq. 2, and c^{id} is the class index. The Integrated Heatmap H^P is obtained by aggregating the PV features and the projected perspective-view feature map:

$$H^P = MLP(F) + F_M^P \quad (4)$$

It is worth noting that F_H is supervised in Heatmap Loss, which will be illustrated in 3.3.

Ultimately, the Integrated Positional Embedding E_I is encoded from the Integrated Heatmap:

$$E_I = MLP(H^P) \quad (5)$$

As a result, E_I is imbued with hybrid cues, enabling it to effectively enhance the subsequent decoding performance.

The visualized samples of Integrated Heatmap in Fig.4 (a) indicate a strong correlation between the distribution of heat intensities and the map instances in the perspective view. For example, higher heat intensities occur near the pedestrian crossing in the left figure and the road boundaries in both figures. Since Integrated Positional Embedding is directly converted from the Integrated Heatmap, it inherently encompasses dependable fused hybrid priors. Therefore, integrating the hybrid features into the formation of positional embedding enforces the decoding to be guided by the high-quality priors from both perspectives, leading to advanced decoding performance on the BEV features.

Enhancement BEV Feature

Within the framework of DEM, the implicit enhancement of BEV features is accomplished through the utilization of the BEV Enhancement Map F_M^B , derived from the BEV features themselves. However, owing to the intrinsic relationship between the enhancement map and the supervised Integrated Heatmap, the BEV Enhancement Map F_M^B undergoes indirect influence, deliberately reinforcing the representation of BEV features. Accordingly, the BEV features are effectively enhanced in an indirect manner, guided by the integration of hybrid inputs.

The implicit enhancement on BEV features is exclusively carried out within the domain of BEV. Given the BEV Enhancement Map derived from Eq. 1, we have the Enhanced BEV features F_E^B by collapsing the F^B and F_M^B :

$$F_E^B = \Psi^1(Cat(F^B, \Omega(F_M^B))) \quad (6)$$

where $\Omega(\cdot)$ is the upsample function and "Cat" indicates concatenation along the feature channel. The Enhanced BEV features $F_E^B \in \mathbb{R}^{H \times W \times C}$ eventually serve as the input feature of the map element decoder.

Fig.4 (b) and (c) visually depict the disparities in the representation of BEV features before and after the implicit enhancement. Compared to the original BEV features in (b), the enhanced BEV features in (c) showcase a more emphasized depiction of map instance information, particularly near the road boundaries and the pedestrian crossing. In terms of results, this selective emphasis on the BEV features through implicit enhancement essentially yields a representation that aligns more closely with the distribution of practical map instances.

3.3 Training Loss

Heatmap Loss. The objective of Heatmap Loss involvement is to deliberately constrain the enhancement process within DEM. As introduced in Sec. 3.2, the Integrated Heatmap H^P is a crucial role in DEM, given its close association with both Integrated Position Embedding and the BEV Enhancement Map. To guarantee the appropriate influence of the hybrid information on H^P , it is supervised by the heatmap formed by the keypoints present in the map vectors.

Given the annotated keypoints projected on perspective-view, the generation of target heatmap H_T^P basically follows the keypoint heatmap in previous object detection methods [Law and Deng, 2018; Duan *et al.*, 2019]. Specifically, we cast all groundtruth keypoints using a Gaussian kernel with constant deviation. The loss \mathcal{L}_H is computed by:

$$\mathcal{L}_H = \mathcal{L}_{Focal}(Sigmoid(H^P), H_T^P) \quad (7)$$

where \mathcal{L}_{Focal} is the focal loss [Lin *et al.*, 2017] between the predicted heatmap and the target.

Rasterized Instance Segmentation Loss. To balance the effects of keypoint emphasis and avoid neglect of trivial points, we introduce the Rasterized Instance Segmentation (RIS) Loss \mathcal{L}_{RIS} into the overall supervision. For a predicted vector \hat{v}_i , we assign the classification score \hat{c}_i to the corresponding pixels to form a BEV mask M_R , while the binary target mask T_R is depicted by groundtruth class labels, represented as one-hot vector c_i . The RIS loss is the cross-entropy loss between the BEV mask and the target mask:

$$\mathcal{L}_{RIS} = \mathcal{L}_{CE}(M^R, M_T^R) \quad (8)$$

Total Loss. Following the previous study [Liao *et al.*, 2022], we leverage focal loss to supervise the category of the predicted vectors, and L1-norm for geometrical properties, whose results are denoted as classification loss \mathcal{L}_{cls} and point-to-point loss \mathcal{L}_{pts} , respectively.

Besides, we inherit the loss combination \mathcal{L}_{BS} from the baseline method [Liao *et al.*, 2023], involving in edge direction loss, auxiliary one2many loss, and auxiliary dense loss. The total loss \mathcal{L}_{total} that participates in the training of HybriMap is

$$\mathcal{L}_{total} = \gamma_H \mathcal{L}_H + \gamma_R \mathcal{L}_{RIS} + \mathcal{L}_{cls} + \mathcal{L}_{pts} + \mathcal{L}_{BS} \quad (9)$$

where γ_H and γ_R are the weighted factors.

4 Experiments

4.1 Experimental Settings

Dataset. We evaluate our method on two popular benchmarks: *nuScenes* [Caesar *et al.*, 2020] and *Argoverse 2* [Wilson *et al.*, 2021]. Each dataset comprises 1000 scenes in total, which are divided into train/validation/test sets with a split of 700/150/150 scenes. In *nuScenes*, each scene contains a video approximately 20s long, where key frames are annotated at 2Hz. These key frames are all captured by 6 surround view onboard cameras with 360 degrees field-of-view, containing 6 images for each. *Argoverse 2* dataset annotates key frames at 10Hz, in which the key frame contains 7 ring cameras.

Metric. Following the previous works [Liu *et al.*, 2023; Liao *et al.*, 2022], we use *Average Precision (AP)* to evaluate the performance of the methods. A predicted instance is defined as true positive only if its Chamfer Distance from the groundtruth is less than a certain threshold. The thresholds are generally defined as $\{0.5m, 1.0m, 1.5m\}$. Meanwhile, we support tighter thresholds $\{0.2m, 0.5m, 1.0m\}$ for a comprehensive comparison with a more precise scale.

Implementation Details. The map instances involves static elements from 3 classes, i.e. pedestrian crossing (*ped*), lane divider (*div*), and road boundary (*bdr*). The perceptual range of the map is defined as the area spanning 15m left and right, as well as 30m front and rear from the ego vehicle. The amount of map vector predictions N_m is set to be 50 and each vector contains 20 points on the BEV plane. The weights of the proposed losses are empirically are set as $\gamma_H = 0.1$ and $\gamma_{RIS} = 15$. Regarding the network, we adopt ResNet50 (R50) [He *et al.*, 2016] as the image backbone and AdamW [Loshchilov and Hutter, 2018] as the optimizer.

4.2 Comparisons with State-of-the-art Methods

Results on *nuScenes*. We compare our results with the existing methods on *nuScenes* dataset, as listed in Tab. 1. Taking results on general thresholds as an example, we achieved appreciable improvements, surpassing the SOTAs by 3.9% *mAP* with 24-epoch training sessions. The results exhibit that our method achieves not only state-of-the-art performance on both threshold sets but also a significantly faster converging speed.

In terms of the obtained results, our method generally demonstrates the most notable improvements in the road boundary class compared to existing methods. This improvement can be attributed to the exploitation of perspective priors to its full extent, as within the three static map elements, road-sides typically exhibit not only prominent color variations but are also surrounded by noticeable ground condition changes, thereby possessing the richest clues from the original inputs.

Results on *Argoverse 2*. To further demonstrate the wide effectiveness of our approach, we present the experimental results on the larger *Argoverse 2*, as shown in Tab. 2. HybriMap gains 2.5% and 5.2% improvement in *mAP* beyond the existing methods, for the two threshold sets respectively. As demonstrated by the experimental results, our method consistently achieves more advanced results in map prediction, both under general and more stringent criteria.

Qualitative Analysis. We present the visualized map construction results under various weather or illumination conditions in Fig. 5. The areas in yellow highlight the discrepancy between map predictions and the corresponding perspective-view clues. Compared with the existing method based on the conventional sequential framework, our HybriMap successfully detects the partition and the sideway along the roadside (e.g. Row 1 and Row 3) as well as the faraway crossing (e.g. Row 2), indicating a more effective utilization of perspective-view hints.

Moreover, due to the mechanism of Heatmap Loss, which supervises the keypoint distribution under perspective-view,

Method	Backbone	Epochs	General Thresholds				Tighter Thresholds			
			AP_{ped}	AP_{div}	AP_{bdr}	mAP	AP_{ped}	AP_{div}	AP_{bdr}	mAP
HDMaNet [2022]	EB0	30	14.4	21.7	33.0	23.0	7.1	28.3	32.6	22.7
VectormapNet [2023]	R50	110	36.1	47.3	39.3	40.9	18.2†	27.2†	18.4†	21.3†
MapTR [2022]	R50	24	46.3	51.5	53.1	50.3	23.2†	30.7†	28.2†	27.3†
BeMapNet [2023]	R50	30	57.7	62.3	59.4	59.8	39.0	46.9	37.8	<u>41.3</u>
PivotNet [2023]	R50	24	56.2	56.5	60.1	57.6	34.3	41.4	<u>39.8</u>	38.5
MapTRv2 [2023]	R50	24	<u>59.8</u>	<u>62.4</u>	<u>62.4</u>	<u>61.5</u>	34.1†	41.6†	36.8†	37.5†
HybriMap	R50	24	63.0	65.9	67.2	65.4	<u>38.1</u>	<u>45.7</u>	42.1	41.9

Table 1: Comparison with SOTA methods on *nuScenes* validation set. "EB0" is the backbone of previous work [Tan and Le, 2019]. "†" indicates the results are re-evaluated by publicly available models. The best and second best results are highlighted in **bold** and underline, respectively.

Method	AP_{ped}	AP_{div}	AP_{bdr}	mAP
VectormapNet [2023]	38.3	36.1	39.2	37.9
MapTRv2 [2023]	62.9	72.1	67.1	67.4
HybriMap	66.6	73.0	70.0	69.9
PivotNet [2023]	31.3	47.5	43.4	40.7
HybriMap	37.9	55.4	44.3	45.9

Table 2: Comparison with SOTA methods on *Argoverse 2* validation set. All the experiment above contains 6-epoch training based on R50 backbone. Results in the top section are evaluated on general thresholds, while in bottom section use tighter thresholds.

our methods can address the issue of incomplete original information caused by occlusion or image blur, to some extent. As shown in Fig. 5 Row 2, the lane divider in the blue shade area is nearly invisible in the raw input. With the combined effect of Integrated Heatmap supervision and feature enhancement, instances in this region have been emphasized and successfully decoded.

However, due to the strong dependence on the original inputs, our approach is limited under the circumstances that PV features are even difficult to extract. For example in Fig. 5 Row 3, the sideways is mispredicted with some directional offset.

4.3 Ablation Studies

Ablation experiments are conducted in this section to analyze the effects of individual modules, including the hybridization of features, DEM, and various loss components. The experiments in this section are trained with R50 backbone through 24 epochs, and evaluated on *nuScenes* validation set on the general threshold set.

Effectiveness of Hybrid Features. In this section, we aim to specify the effectiveness of hybrid features through comparative experiments. Concerning the fact that the implicit enhancement on BEV features themselves is depended on the hybrid features, we take positional embedding as the example to compare the impact of encoding based on pure PV features or hybrid features on the map estimation results. As listed in Tab. 3, the positional embedding encoded by hybrid features achieves 0.9% mAP higher than that from pure PV features. The results demonstrate that the involvement of BEV features is capable of providing significant referential information, regarding the re-utilization of PV features.

PE Mode	AP_{ped}	AP_{div}	AP_{bdr}	mAP
PV	60.9	62.8	66.2	63.3
Hybrid	61.9	64.7	66.0	64.2

Table 3: Comparison between pure PV features and Hybrid features regarding positional embedding mode. The column "PE Mode" indicates the positional embedding is encoded by pure PV features (Row 1) or hybrid features (Row 2).

Exp.	Int.	Enh.	AP_{ped}	AP_{div}	AP_{bdr}	mAP
0			59.7	62.3	64.9	62.3
1	✓		61.9	64.7	66.0	64.2
2		✓	60.9	63.5	65.5	63.3
3	✓	✓	63.0	65.9	67.2	65.4

Table 4: Ablation studies of DEM. "Int." and "Enh." represent the participation of Integrated Positional Embedding and implicit Enhancement on BEV features, respectively.

Effectiveness of Dual Enhancement Module. In order to assess the efficacy of the dual enhancement, we perform individual experiments on the two outputs generated by the DEM, namely Integrated Positional Embedding and implicitly Enhanced BEV features. The experimental results, presented in Tab. 4, demonstrate the impact of explicit integration on positional embedding and BEV enhancement. These enhancements lead to improvements of 1.9% and 1.0% in mAP , respectively, in the final results. Moreover, the dual enhancement can leverage the advantages of both enhancement branches, resulting in a significant mAP improvement of 3.1%.

Effectiveness of Loss Components. We further verify the impacts of the proposed losses, i.e. Heatmap Loss and RIS Loss, as demonstrated in Tab. 5. Under the joint influence of \mathcal{L}_H and \mathcal{L}_{RIS} , the overall results attain a 1.7% increase in mAP .

4.4 Extended task: 3D Map Construction

HybriMap demonstrates its capability in 3D map construction by elevating the dimension of map vectors to 3-dimensional space. The experiment on 3D map construction is presented in Table 6, conducted on the validation set of *Argoverse 2*, with evaluation based on AP using general thresholds. The results clearly indicate a notable improvement (3.8% mAP)

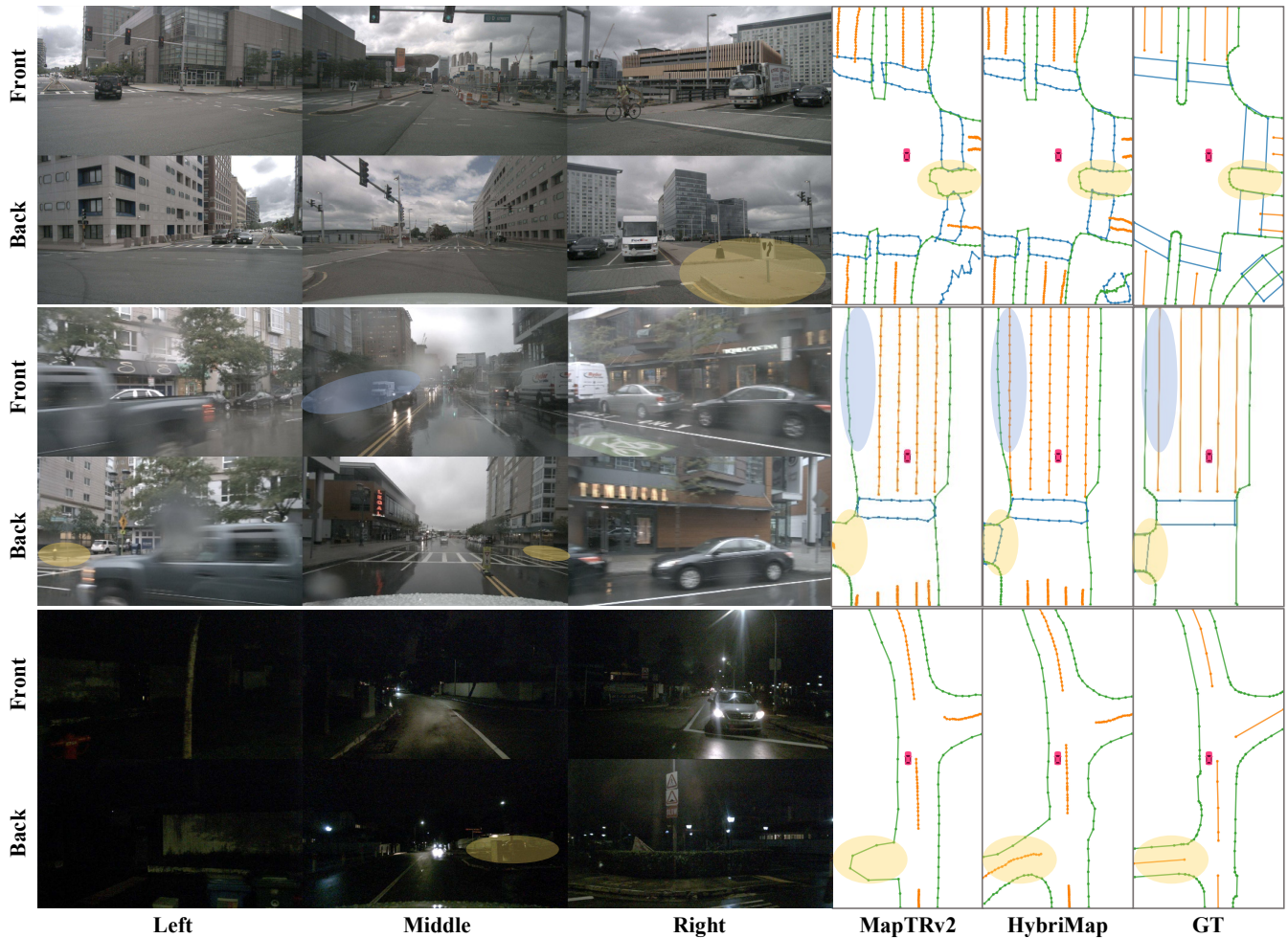


Figure 5: **Qualitative results on *nuScenes* validation dataset.** We provide the complete surround view inputs, predictions of MapTRv2[Liao *et al.*, 2023], HybriMap, and the ground truth map. The regions that are highlighted by colored ellipses enclose instances that are difficult to detect.

Exp.	\mathcal{L}_H	\mathcal{L}_{RIS}	AP_{ped}	AP_{div}	AP_{bdr}	mAP
0			62.1	64.0	65.0	63.7
1	✓		62.8	65.0	65.5	64.4
2		✓	60.9	65.2	66.7	64.3
3	✓	✓	63.0	65.9	67.2	65.4

Table 5: Ablation studies of loss components.

achieved by our method. This significant advancement can be attributed to the influential role of PV features, which facilitate the integration of height information into BEV features and enable their effective decoding as 3D map vectors. The results of this experiment indicate that our method can maintain its superiority in the derivative task.

5 Conclusion

In this paper, we propose HybriMap to address the issue of information loss in HD map construction. In particular, we design a hybrid approach to effectively re-utilize the

Method	AP_{ped}	AP_{div}	AP_{bdr}	mAP
VectormapNet [2023]	36.5	35.0	36.2	35.8
MapTRv2 [2023]	60.7	68.9	64.5	64.7
HybriMap	64.0	72.5	69.1	68.5

Table 6: Experimental results of 3D map construction. Our HybridMap framework exhibits applicability in 3D map vector prediction, showcasing significant advancements compared to previous studies.

perspective-view features from the original inputs. Furthermore, the Dual Enhancement Module is employed to enhance both the decoding performance and the BEV representation, simultaneously. Extensive experiments on the dataset have demonstrated the superiority of our method, achieving SOTA performance in HD map construction. Furthermore, our method can be effectively applied to the derivative task. We anticipate that the aforementioned research can provide more reliable map support for autonomous driving and contribute to future investigations in HD map studies.

References

- [Caesar *et al.*, 2020] Holger Caesar, Varun Bankiti, Alex H Lang, Sourabh Vora, Venice Erin Liong, Qiang Xu, Anush Krishnan, Yu Pan, Giancarlo Baldan, and Oscar Beijbom. nuscenes: A multimodal dataset for autonomous driving. In *Proceedings of the IEEE/CVF conference on computer vision and pattern recognition*, pages 11621–11631, 2020.
- [Can *et al.*, 2022] Yigit Baran Can, Alexander Liniger, Danda Pani Paudel, and Luc Van Gool. Topology preserving local road network estimation from single onboard camera image. In *Proceedings of the IEEE/CVF Conference on Computer Vision and Pattern Recognition*, pages 17263–17272, 2022.
- [Carion *et al.*, 2020] Nicolas Carion, Francisco Massa, Gabriel Synnaeve, Nicolas Usunier, Alexander Kirillov, and Sergey Zagoruyko. End-to-end object detection with transformers. In *European conference on computer vision*, pages 213–229. Springer, 2020.
- [Conde *et al.*, 2023] Marcos V Conde, Rafael Barea, Luis M Bergasa, and Carlos Gómez-Huélamo. Improving multi-agent motion prediction with heuristic goals and motion refinement. In *Proceedings of the IEEE/CVF Conference on Computer Vision and Pattern Recognition*, pages 5322–5331, 2023.
- [Da and Zhang, 2022] Fang Da and Yu Zhang. Path-aware graph attention for hd maps in motion prediction. In *2022 International Conference on Robotics and Automation (ICRA)*, pages 6430–6436. IEEE, 2022.
- [Diaz-Diaz *et al.*, 2022] Alejandro Diaz-Diaz, Manuel Ocaña, Ángel Llamazares, Carlos Gómez-Huélamo, Pedro Revenga, and Luis M Bergasa. Hd maps: Exploiting opendrive potential for path planning and map monitoring. In *2022 IEEE Intelligent Vehicles Symposium (IV)*, pages 1211–1217. IEEE, 2022.
- [Ding *et al.*, 2023] Wenjie Ding, Limeng Qiao, Xi Qiu, and Chi Zhang. Pivotnet: Vectorized pivot learning for end-to-end hd map construction. In *Proceedings of the IEEE/CVF International Conference on Computer Vision (ICCV)*, pages 3672–3682, October 2023.
- [Duan *et al.*, 2019] Kaiwen Duan, Song Bai, Lingxi Xie, Honggang Qi, Qingming Huang, and Qi Tian. Centernet: Keypoint triplets for object detection. In *Proceedings of the IEEE/CVF international conference on computer vision*, pages 6569–6578, 2019.
- [Gao *et al.*, 2020] Jiyang Gao, Chen Sun, Hang Zhao, Yi Shen, Dragomir Anguelov, Congcong Li, and Cordelia Schmid. Vectornet: Encoding hd maps and agent dynamics from vectorized representation. In *Proceedings of the IEEE/CVF Conference on Computer Vision and Pattern Recognition*, pages 11525–11533, 2020.
- [Gehring *et al.*, 2017] Jonas Gehring, Michael Auli, David Grangier, Denis Yarats, and Yann N Dauphin. Convolutional sequence to sequence learning. In *International conference on machine learning*, pages 1243–1252. PMLR, 2017.
- [He *et al.*, 2016] Kaiming He, Xiangyu Zhang, Shaoqing Ren, and Jian Sun. Deep residual learning for image recognition. In *Proceedings of the IEEE conference on computer vision and pattern recognition*, pages 770–778, 2016.
- [Jian *et al.*, 2019] Zhiqiang Jian, Songyi Zhang, Shitao Chen, Xin Lv, and Nanning Zheng. High-definition map combined local motion planning and obstacle avoidance for autonomous driving. In *2019 IEEE Intelligent Vehicles Symposium (IV)*, pages 2180–2186. IEEE, 2019.
- [Law and Deng, 2018] Hei Law and Jia Deng. Cornernet: Detecting objects as paired keypoints. In *Proceedings of the European conference on computer vision (ECCV)*, pages 734–750, 2018.
- [Li *et al.*, 2022] Qi Li, Yue Wang, Yilun Wang, and Hang Zhao. Hdmapnet: An online hd map construction and evaluation framework. In *2022 International Conference on Robotics and Automation (ICRA)*, pages 4628–4634. IEEE, 2022.
- [Liao *et al.*, 2022] Bencheng Liao, Shaoyu Chen, Xinggang Wang, Tianheng Cheng, Qian Zhang, Wenyu Liu, and Chang Huang. Maptr: Structured modeling and learning for online vectorized hd map construction. In *The Eleventh International Conference on Learning Representations*, 2022.
- [Liao *et al.*, 2023] Bencheng Liao, Shaoyu Chen, Yunchi Zhang, Bo Jiang, Qian Zhang, Wenyu Liu, Chang Huang, and Xinggang Wang. Maptrv2: An end-to-end framework for online vectorized hd map construction. *arXiv preprint arXiv:2308.05736*, 2023.
- [Lin *et al.*, 2017] Tsung-Yi Lin, Priya Goyal, Ross Girshick, Kaiming He, and Piotr Dollár. Focal loss for dense object detection. In *Proceedings of the IEEE international conference on computer vision*, pages 2980–2988, 2017.
- [Liu *et al.*, 2023] Yicheng Liu, Tianyuan Yuan, Yue Wang, Yilun Wang, and Hang Zhao. Vectormapnet: End-to-end vectorized hd map learning. In *International Conference on Machine Learning*, pages 22352–22369. PMLR, 2023.
- [Loshchilov and Hutter, 2018] Ilya Loshchilov and Frank Hutter. Decoupled weight decay regularization. In *International Conference on Learning Representations*, 2018.
- [Pillion and Fidler, 2020] Jonah Pillion and Sanja Fidler. Lift, splat, shoot: Encoding images from arbitrary camera rigs by implicitly unprojecting to 3d. In *Proceedings of the European Conference on Computer Vision*, 2020.
- [Qiao *et al.*, 2023] Limeng Qiao, Wenjie Ding, Xi Qiu, and Chi Zhang. End-to-end vectorized hd-map construction with piecewise bezier curve. In *Proceedings of the IEEE/CVF Conference on Computer Vision and Pattern Recognition*, pages 13218–13228, 2023.
- [Roddick and Cipolla, 2020] Thomas Roddick and Roberto Cipolla. Predicting Semantic Map Representations From Images Using Pyramid Occupancy Networks. In *2020 IEEE/CVF Conference on Computer Vision and Pattern Recognition (CVPR)*, pages 11135–11144, Seattle, WA, USA, June 2020. IEEE.

- [Tan and Le, 2019] Mingxing Tan and Quoc Le. EfficientNet: Rethinking Model Scaling for Convolutional Neural Networks. In Kamalika Chaudhuri and Ruslan Salakhutdinov, editors, *Proceedings of the 36th International Conference on Machine Learning*, volume 97 of *Proceedings of Machine Learning Research*, pages 6105–6114. PMLR, June 2019.
- [Wilson *et al.*, 2021] Benjamin Wilson, William Qi, Tanmay Agarwal, John Lambert, Jagjeet Singh, Siddhesh Khandelwal, Bowen Pan, Ratnesh Kumar, Andrew Hartnett, Jhony Kaesemodel Pontes, Deva Ramanan, Peter Carr, and James Hays. Argoverse 2: Next generation datasets for self-driving perception and forecasting. In *Proceedings of the Neural Information Processing Systems Track on Datasets and Benchmarks (NeurIPS Datasets and Benchmarks 2021)*, 2021.
- [Yang *et al.*, 2021] Weixiang Yang, Qi Li, Wenxi Liu, Yuanlong Yu, Yuexin Ma, Shengfeng He, and Jia Pan. Projecting your view attentively: Monocular road scene layout estimation via cross-view transformation. In *Proceedings of the IEEE/CVF conference on computer vision and pattern recognition*, pages 15536–15545, 2021.
- [Yang *et al.*, 2023] Chenyu Yang, Yuntao Chen, Hao Tian, Chenxin Tao, Xizhou Zhu, Zhaoxiang Zhang, Gao Huang, Hongyang Li, Yu Qiao, Lewei Lu, et al. Bevformer v2: Adapting modern image backbones to bird’s-eye-view recognition via perspective supervision. In *Proceedings of the IEEE/CVF Conference on Computer Vision and Pattern Recognition*, pages 17830–17839, 2023.
- [Yu *et al.*, 2023] Jingyi Yu, Zizhao Zhang, Shengfu Xia, and Jizhang Sang. Scalablemap: Scalable map learning for online long-range vectorized hd map construction. In *7th Annual Conference on Robot Learning*, 2023.
- [Yuan *et al.*, 2024] Tianyuan Yuan, Yicheng Liu, Yue Wang, Yilun Wang, and Hang Zhao. Streammapnet: Streaming mapping network for vectorized online hd map construction. In *Proceedings of the IEEE/CVF Winter Conference on Applications of Computer Vision*, pages 7356–7365, 2024.
- [Zhou and Krähenbühl, 2022] Brady Zhou and Philipp Krähenbühl. Cross-view transformers for real-time map-view semantic segmentation. In *Proceedings of the IEEE/CVF conference on computer vision and pattern recognition*, pages 13760–13769, 2022.
- [Zhu *et al.*, 2020] Xizhou Zhu, Weijie Su, Lewei Lu, Bin Li, Xiaogang Wang, and Jifeng Dai. Deformable detr: Deformable transformers for end-to-end object detection. In *International Conference on Learning Representations*, 2020.

Supplementary Material

1 Additional Experiments

2 To showcase the efficiency of HybriMap inference, we
3 present the frames per second (FPS) results of various meth-
4 ods, as detailed in Tab. 1. All FPS evaluations are performed
5 on a single NVIDIA RTX 3090 GPU. The findings reveal that
6 the accuracy enhancement offered by HybriMap does not sig-
7 nificantly compromise its efficiency, as evidenced by a mere
8 0.8 FPS reduction accompanied by a 3.9% *mAP* improve-
9 ment.

Method	Backbone	<i>mAP</i>	FPS
MapTR [?]	R50	50.3	14.0 †
MapTRv2 [?]	R50	61.5	10.7†
HybriMap	R50	65.4	9.9

Table 1: FPS comparison of existing methods. Results with "†" are re-evaluated based on publicly available codes.

10 2 Additional Visualized Results

11 We provide additional visualized results on the *nuScenes* and
12 *Argoverse 2* datasets. Fig. 1 showcases predicted samples
13 from the *nuScenes* dataset, illustrating scenes captured under
14 diverse weather and illumination conditions. Fig. 2 demon-
15 strates the visualized results of HD map construction on the
16 *Argoverse 2* dataset. Since no publicly available models
17 trained on this specific dataset have been released, the quali-
18 tative comparison to existing methods has been omitted. The
19 presented visual samples demonstrate the reliability of HD
20 map constructed by our HybriMap under various conditions.

21 To illustrate the applicability of the proposed method to
22 the derivative task, we further provide the visualized results
23 of 3D map construction, as demonstrated in Fig. 3. To exhibit
24 the accuracy of the map construction in the three-dimensional
25 space, 3D map vectors are projected to and presented in both
26 PV and BEV. The visualized samples showcase that the pre-
27 dicted 3D map vectors are closely aligned with the raw input
28 data and accurately capture the map structures.

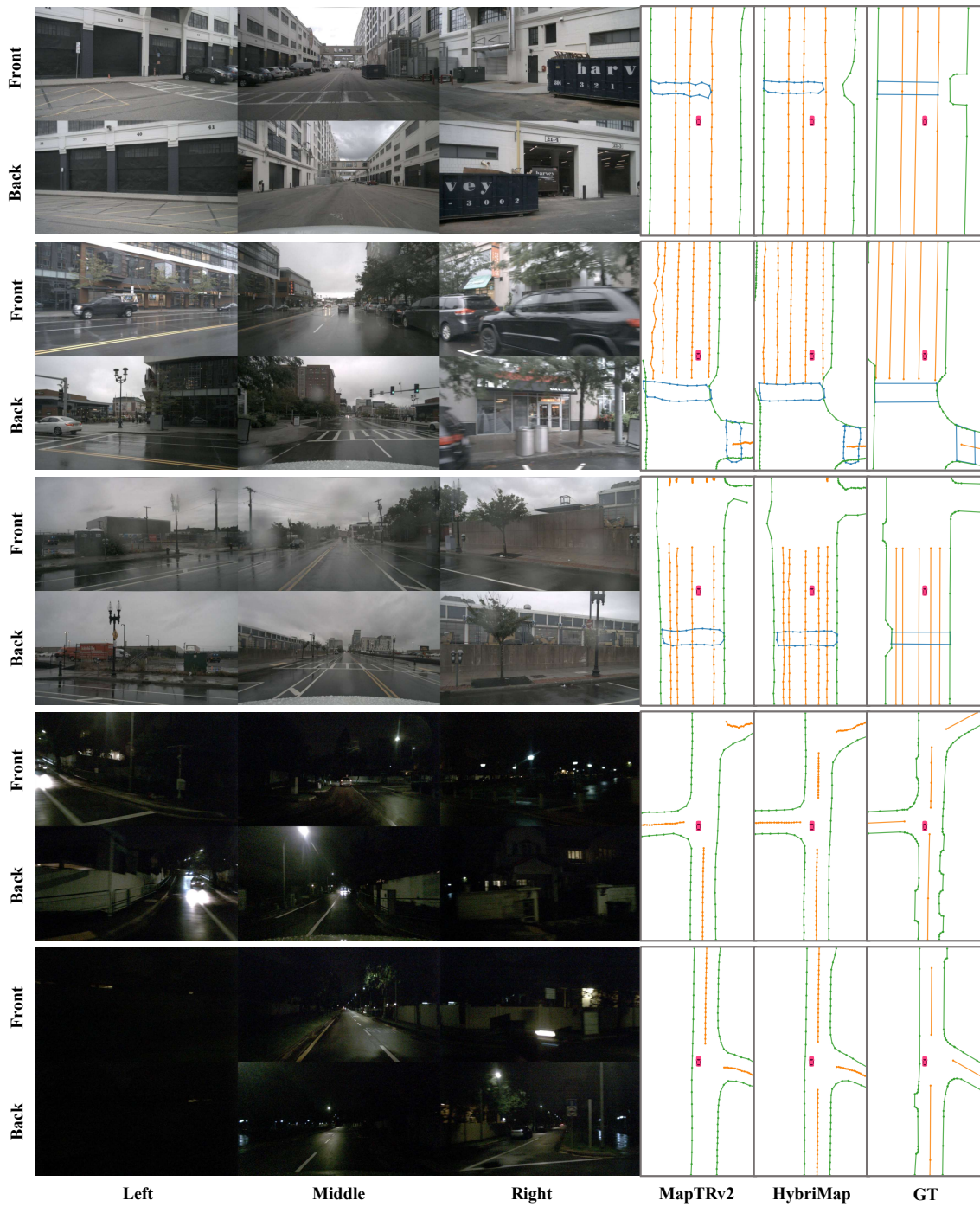
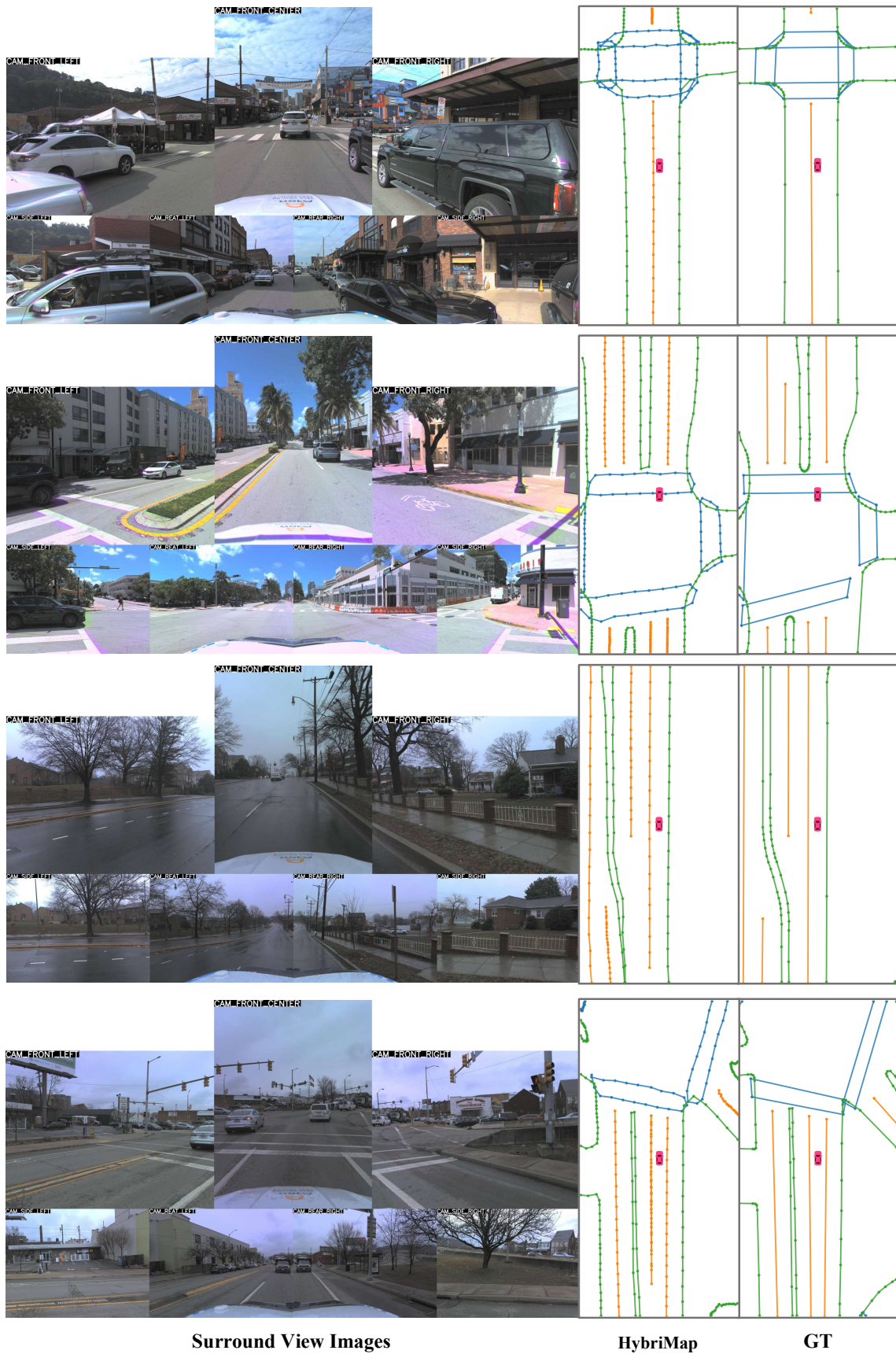


Figure 1: Visualized results on *nuScenes* validation dataset.

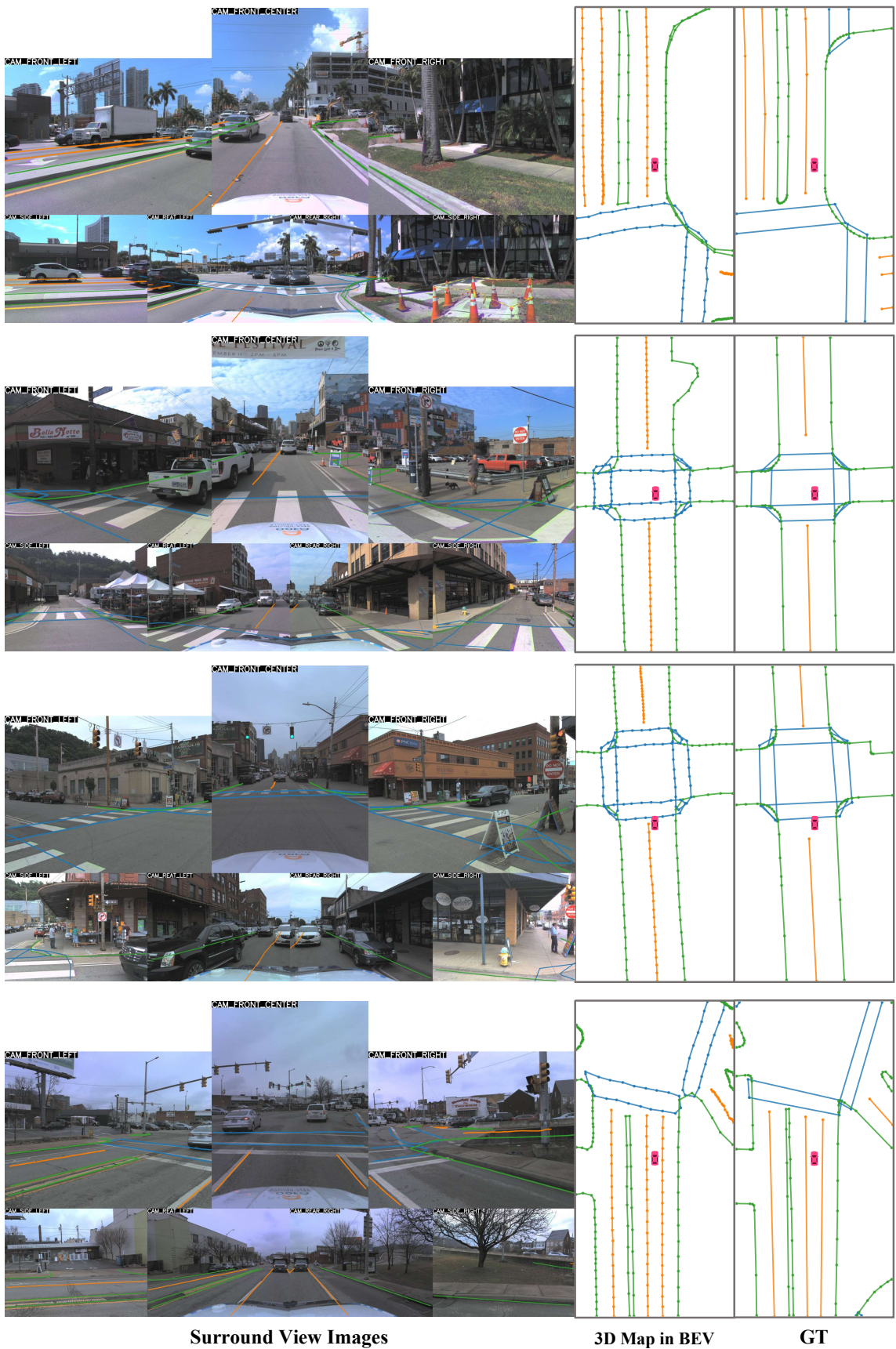


Surround View Images

HybriMap

GT

Figure 2: Visualized results on *Argoverse 2* validation dataset.



Surround View Images

3D Map in BEV

GT

Figure 3: 3D map construction results on Argoverse 2 validation dataset.